Neutron-proton mass splitting and pygmy dipole resonance in ^{208}Pb

Xuwei Sun, Jing Chen, and Dinghui Lu
Department of Physics, Zhejiang University, 310027 Hangzhou, China

(Received 26 January 2019; revised manuscript received 18 March 2019; published 3 May 2019)

The pygmy dipole resonance (PDR) of ^{208}Pb is studied with random phase approximation method. The effect of the neutron-proton mass splitting is discussed in the framework of relativistic mean field theory via including the scalar-isovector meson δ explicitly. The model is calibrated with nuclear bulk properties as well as finite nuclei data, and is further checked by terrestrial experimental and astrophysical constraints. The inclusion of δ meson reduces the neutron skin thickness of ^{208}Pb as well as ^{48}Ca, which are turned out to be closely related. The energy of pygmy dipole resonance is in a large extent dominated by the excitations of neutrons near the Fermi surface. We found that the peak positions of the giant dipole resonance (GDR) and the PDR are sensitive to the nucleon-meson coupling in the scalar-isovector channel. A linear correlation between the neutron-proton effective mass splitting at saturation density and the relative offset of GDR and PDR is identified in ^{208}Pb.

DOI: 10.1103/PhysRevC.99.054604

I. INTRODUCTION

The relativistic mean field (RMF) theory is widely used in nuclear investigations [1,2]. The meson-exchange-type RMF model was first proposed by Walecka [3]. The nucleons move independently in a mean field provided by the cancellation between scalar σ and vector ω^μ meson fields. The isospin asymmetry is treated via an effective $\vec{\rho}^\mu$ meson [4]. By adjusting the coupling constants, one can make the nuclear matter saturated appropriately. In quantitative applications, it is realized that the inclusions of the self or cross couplings between various mesons are necessary. For example, the electron fraction Y_e for the uniform neutron-rich matter in β equilibrium depends on the cross coupling between ω and $\vec{\rho}^\mu$ mesons [5]. The $\vec{\delta}$ meson, which is the counterpart of $\vec{\rho}^\mu$ meson in the isospin space, is often omitted in some relativistic meson-exchange models in order to reduce the number of the adjustable parameters. However, there are already some researches suggested that the scalar-isovector meson $\vec{\delta}$ plays significant roles in the asymmetric nuclear matter [6] and compact stars [7]. The inclusion of the $\vec{\delta}$ meson increases the neutrino emissivity in direct Urca process in neutron star cooling [8]. One unique effect of $\vec{\delta}$ meson is to split the neutron-proton effective mass.

In nonrelativistic models the effective mass of a nucleon measures the nonlocality and the momentum dependence of the single-particle potential in nuclear medium. It has been reported that in ^{208}Pb the effective mass is linearly correlated with the energy weighted sum rule (EWSR) m_1 of the isovector giant dipole resonance (IVGDR). Therefore, from the experimental value of m_1, the effective nucleon mass in symmetric nuclear matter at saturation density is determined as $m^*/m = 0.77 \pm 0.03$ [9]. The splitting of the effective mass is thought to be sensitive to the neutron/proton ratio in the early universe and will affect the nucleus-nucleus reaction dynamics [10]. Attempts have been made to constrain the neutron-proton effective mass splitting via nucleon-nucleus scattering data [11] and nucleus giant resonances [12]. However, up to now it is still opaque and even the sign of the splitting has not been determined [13]. In relativistic approaches an additional effective mass exists, namely, the Dirac mass [14]. It characterizes the Lorentz transformation property of the scalar potential and typically has a low value [15]. The effective mass has an important influence on the nucleon single-particle states. It has been shown that the energy-dependent effective mass, which means correcting the scalar and vector potentials with a linear density dependence, can significantly increase the states density around the Fermi surface, and achieve a better agreement with experimental single nucleon spectra [16]. The response of a nucleus to external perturbations is sensitive to the single-particle spectra and studying them are important approaches to reveal the nuclear structure and interaction details.

The centroid energy of the isoscalar giant monopole resonance (ISGMR) is proportional to the square root of the finite nucleus compression modulus K_A [17]. The resonance structures, such as the giant dipole resonance (GDR), in spherical nuclei are closely related to the symmetry energy [18], as is the pygmy dipole resonance (PDR) [19,20]. PDR emerges as the electric dipole strength near the particle separation threshold in neutron-rich nucleus [21–25], which draws more and more attentions from experimental studies [26] and theoretical investigations [27]. PDR usually exhausts only a few percent of the integrated strength, and sometimes one needs to separate it from the low-energy tail of GDR and other low-lying structures, such as the magnetic dipole ($M1$) resonance [28]. PDR is important to neutron capture rate and nucleosynthesis [29]. Basically, in neutron-rich isotopes the PDR strength increases with neutron-to-proton ratios, but the evolution also exhibits specific shell effects [30,31]. Recently, intense discussions are made to illustrate its collectivity [31,32], relationship with the neutron skin thickness

[30,33–35], and the deformation [36,37]. The GDR manifests the relative motion between neutrons and protons, hence is of isovector nature. In contrast, PDR is caused by the oscillation of the excess neutrons against an inert core and exhibits some isoscalar character [38]. The isoscalar dominance of PDR is suggested by previous studies using Skyrme interactions [39,40], and is manifested as its close connection with the low-lying isoscalar torus mode [41]. Meanwhile, the different results from $(\alpha, \alpha'\gamma)$ and (γ, γ') reactions indicate that PDR splits into isoscalar and isovector components [42–44], implying fine structures exist in PDR. In addition to the electromagnetic probe [45–47], other experimental approaches have been considered, such as studying PDR through decay patterns [48,49]. Given the complexity of the issues, investigating the effect of isospin asymmetry on PDR, such as revealing the possible correlation between neutron-proton mass splitting and PDR, will be beneficial.

II. THEORETICAL FRAMEWORK

The interaction between nucleons are described by exchanging various mesons, including the scalar meson σ, the vector meson ω^μ, the scalar-isovector meson $\vec{\delta}$, and the vector-isovector meson $\vec{\rho}^\mu$. The Lagrangian density of the whole nuclear system reads

$$\mathcal{L} = \mathcal{L}_0 + \mathcal{L}_{\rm int}. \tag{1}$$

$\mathcal{L}_{\rm int}$ is the interacting part, generally, it can be expressed as

$$\begin{aligned}\mathcal{L}_{\rm int} = &-\bar{\psi}\{(g_\sigma\sigma + g_\delta\vec{\delta}\cdot\vec{\tau}) + \gamma_\mu(g_\omega\omega^\mu + g_\rho\vec{\rho}^\mu\cdot\vec{\tau})\}\psi \\ &- e\bar{\psi}\frac{1+\tau_3}{2}\gamma_\mu A^\mu\psi - U(\sigma,\omega^\mu,\vec{\delta},\vec{\rho}^\mu).\end{aligned} \tag{2}$$

The nonlinear interactions include various self or/and cross couplings of meson fields,

$$\begin{aligned}U(\sigma,\omega^\mu,\vec{\delta},\vec{\rho}^\mu) = &\tfrac{1}{3}g_2\sigma^3 + \tfrac{1}{4}g_3\sigma^4 + \tfrac{1}{4}c_0(\omega^\mu\omega_\mu)^2 \\ &+ \tfrac{1}{2}S_a\sigma^2\vec{\delta}^2 + \tfrac{1}{2}S_b\omega^\mu\omega_\mu\vec{\delta}^2 \\ &+ \tfrac{1}{2}T_a\sigma^2\vec{\rho}^\mu\vec{\rho}_\mu + \tfrac{1}{2}T_b\omega^\mu\omega_\mu\vec{\rho}^\mu\vec{\rho}_\mu \\ &+ \ldots.\end{aligned} \tag{3}$$

Typically, some of the terms are substitutable and not all of them appear in a model. The self-interactions of σ meson as well as that of ω meson are crucial. The former are essential to reduce the incompressibility of symmetric nuclear matter [50], while the latter softens the equation of state (EoS) in the high-density region [51]. On the contrary, the cross couplings involving isovector mesons $\vec{\delta}$ and $\vec{\rho}^\mu$ are usually omitted, partially because their effects are quantitatively small when the magnitudes of the coupling constants are the same order as direct coupling terms, especially in the vicinity of the saturation density. However, strong ω_μ-$\vec{\rho}^\mu$ coupling will soften the EoS prominently [52]. Similarly, the couplings between σ-$\vec{\delta}$ and ω^μ-$\vec{\delta}$ mesons may be helpful to reveal the isospin dependence of the effective nuclear interaction. The equation of motion of the nucleon or the meson field ϕ_i can be obtained from the Euler-Lagrangian equation

$$\partial_\mu\frac{\partial\mathcal{L}}{\partial(\partial_\mu\phi_i)} - \frac{\partial\mathcal{L}}{\partial\phi_i} = 0. \tag{4}$$

The Dirac equation for the nucleon is

$$[\gamma_\mu(i\partial^\mu - V^\mu) - M^*]\psi = 0, \tag{5}$$

where the effective mass and the vector potential are

$$\begin{aligned}M^* &= M + g_\sigma\sigma + g_\delta\vec{\delta}\cdot\vec{\tau}, \\ V^\mu &= g_\omega\omega^\mu + g_\rho\vec{\rho}^\mu\cdot\vec{\tau} + e\frac{1+\tau_3}{2}A^\mu.\end{aligned} \tag{6}$$

The Klein-Gordon equations for meson fields read

$$\begin{aligned}(-\Delta + m_\sigma^2)\sigma &= -g_\sigma\bar{\psi}\psi - \frac{\partial U}{\partial\sigma}, \\ (-\Delta + m_\omega^2)\omega^\mu &= g_\omega\bar{\psi}\gamma^\mu\psi + \frac{\partial U}{\partial\omega_\mu}, \\ (-\Delta + m_\delta^2)\vec{\delta} &= -g_\delta\bar{\psi}\vec{\tau}\psi - \frac{\partial U}{\partial\vec{\delta}}, \\ (-\Delta + m_\rho^2)\vec{\rho}^\mu &= g_\rho\bar{\psi}\vec{\tau}\gamma^\mu\psi + \frac{\partial U}{\partial\vec{\rho}_\mu}.\end{aligned} \tag{7}$$

The Hamiltonian density can be derived from the energy-momentum tensor as

$$\mathcal{H} = \mathcal{T}^{00} = \frac{\partial\mathcal{L}}{\partial\dot{\phi}_i}\dot{\phi}_i - \mathcal{L}. \tag{8}$$

For nuclear systems such as the infinite nuclear matter as well as the even-even nuclei, the contributions of space components of the vector mesons vanish. In addition, if there is no isospin mixing, the remaining components of the meson fields contributing to the energy are ω^0, ρ_3^0, and δ_3. For simplicity, in the following we use the simplification $\delta \to \delta_3$, $\omega \to \omega^0$, $\rho \to \rho_3^0$, and the nonlinear interaction $U(\sigma,\omega^\mu,\vec{\delta},\vec{\rho}^\mu)$ is simplified as $U(\sigma,\omega,\delta,\rho)$. The scalar, vector, scalar-isovector, vector-isovector densities are, correspondingly,

$$\begin{aligned}\rho_s &= \langle\bar{\psi}\psi\rangle, \quad \rho_v = \langle\bar{\psi}\gamma^0\psi\rangle, \\ \rho_{st} &= \langle\bar{\psi}\tau_3\psi\rangle, \quad \rho_{vt} = \langle\bar{\psi}\tau_3\gamma^0\psi\rangle,\end{aligned} \tag{9}$$

where the brackets represent taking the expectation values. Then the total energy $E = \langle\int\mathcal{H}d^3r\rangle$ can be simply denoted as

$$E = \langle\boldsymbol{\alpha}\cdot\boldsymbol{p}\rangle + \frac{1}{2}\sum_\phi\left\langle g_\phi\rho_\phi\phi - \frac{\partial U}{\partial\phi}\phi\right\rangle + \langle U\rangle, \tag{10}$$

with $\phi = \{\sigma,\omega^0,\delta_3,\rho_3^0\}$ and $\rho_\phi = \{\rho_s,\rho_v,\rho_{st},\rho_{vt}\}$. $\langle\boldsymbol{\alpha}\cdot\boldsymbol{p}\rangle$ represents the kinetic term, where $\boldsymbol{\alpha} = \gamma^0\boldsymbol{\gamma}$. The charge radius is calculated from the proton distributions by accounting the finite-size effects of proton [53]

$$r_c = \sqrt{\langle\hat{r}\rangle_p^2 + 0.64} \quad \text{(fm)}. \tag{11}$$

For asymmetric nuclear matter, the binding energy can be expressed as

$$E(\rho,\alpha) = E(\rho,0) + E_{\rm sym}(\rho)\alpha^2 + O(\alpha^4), \tag{12}$$

where $\alpha \equiv (\rho_n - \rho_p)/\rho$ is the asymmetry coefficient, or the neutron excess ratio. $E_{\rm sym}$ is the symmetry energy, which can be expanded near the saturation density ρ_0:

$$E_{\rm sym}(\rho) = E_{\rm sym}(\rho_0) + \frac{L_{\rm sym}}{3}\left(\frac{\rho-\rho_0}{\rho_0}\right) + \frac{K_{\rm sym}}{18}\left(\frac{\rho-\rho_0}{\rho_0}\right)^2. \tag{13}$$

The slope and curvature parameters of symmetry energy are defined as

$$L_{\rm sym} \equiv 3\rho_0 \frac{\partial E_{\rm sym}}{\partial \rho}\bigg|_{\rho=\rho_0}, \quad K_{\rm sym} \equiv 9\rho_0^2 \frac{\partial^2 E_{\rm sym}}{\partial \rho^2}\bigg|_{\rho=\rho_0}. \tag{14}$$

In this investigation, the random phase approximation (RPA) is used to calculate the low lying excitation properties. This method is very useful for small amplitude oscillations and are intensely used in nuclear researches [54–58], and many specific techniques have been developed [59–62]. The low-lying excitation is approximated by the coherent transitions of one-particle one-hole (1p1h) pairs,

$$|\nu\rangle = \sum_{ph}\left(X^{\nu}_{ph}a^{\dagger}_{p}a_{h} - Y^{\nu}_{ph}a^{\dagger}_{h}a_{p}\right)|0\rangle. \tag{15}$$

X^{ν}_{ph} and Y^{ν}_{ph} are the matrix elements of the transition density, which can be obtained by solving the RPA equation [63]

$$\begin{pmatrix} A & B \\ B^* & A^* \end{pmatrix}\begin{pmatrix} X \\ Y \end{pmatrix} = \omega\begin{pmatrix} 1 & 0 \\ 0 & -1 \end{pmatrix}\begin{pmatrix} X \\ Y \end{pmatrix}, \tag{16}$$

where the matrix elements of A and B are

$$\begin{aligned} A_{php'h'} &= \langle [a^{\dagger}_{h}a_{p}, [\hat{H}, a^{\dagger}_{p'}a_{h'}]]\rangle, \\ B_{php'h'} &= -\langle [a^{\dagger}_{h}a_{p}, [\hat{H}, a^{\dagger}_{h'}a_{p'}]]\rangle. \end{aligned} \tag{17}$$

Again, the angle brackets represent taking the expectation values in the mean field ground state. Taking the electric dipole operator $\hat{E}_{1\mu}$ as an example, the reduced transition probability from the RPA ground state $|0\rangle$ to an excited state $|\nu\rangle$ is given by

$$\begin{aligned} B(\hat{E}_1; 0 \to \nu) &= |\langle \nu||\hat{E}_1||0\rangle|^2 \\ &= \left|\sum_{ph}\left(X^{\nu}_{ph} + Y^{\nu}_{ph}\right)\langle p||\hat{E}_1||h\rangle\right|^2. \end{aligned} \tag{18}$$

In order to get a continuous strength distribution, the transition probabilities of discrete RPA states ω_ν are folded via a Lorentzian function

$$\frac{dB(\hat{E}_1;\omega)}{d\omega} = \frac{1}{\pi}\sum_{\nu} B(\hat{E}_1; 0 \to \nu)\frac{\Gamma/2}{(\omega-\omega_\nu)^2 + (\Gamma/2)^2}. \tag{19}$$

The kth moment of the electric dipole operator is defined by [63]

$$m_k \equiv \sum_{\nu} \omega^k_{\nu} B(\hat{E}_1; 0 \to \nu). \tag{20}$$

III. χ^2 MINIMIZATION OF THE MODEL PARAMETERS

The model parameters are calibrated using the bulk properties of the infinite nuclear matter as well as finite nuclei data. In the vicinity of the saturation density and with mild neutron excess, the nuclei data are excellent benchmarks to constrain the theoretical models. The fitting data contain the averaged nucleon masses [64] and the charge radii [65] of some double-closed nuclei, i.e., ^{40}Ca, ^{48}Ca, and ^{208}Pb. As for the bulk properties, we follow Ref. [66], namely, taking the empirical values and the errors of the saturation density, the averaged binding energy, the incompressibility and the symmetry energy as $\rho_0 = 0.153(10\%)$, $E/A = -16(5\%)$, $K_0 = 250(10\%)$, $E_{\rm sym} = 33(10\%)$. Least-squares fitting proceeds as follows. First, the scaled least square χ^2 is defined as

$$\chi^2 = \frac{1}{n}\sum_{i}^{n} w_i^2\left(\frac{O_i^{\rm fit.}}{O_i^{\rm exp.}} - 1\right)^2, \tag{21}$$

where the weight factor w_i of the ith observable is defined via the uncertainty of the corresponding experimental measurement or empirical values

$$w_i \equiv \ln\frac{O_i^{\rm exp.}}{\Delta O_i^{\rm exp.}}. \tag{22}$$

The reason for including a logarithm function in the definition of the weight factor is that the masses of the finite nuclei are always measured very precisely, as are the charge radii. Therefore, using experimental errors directly will make the constraints from the finite data extremely strong, and make that from the empirical values irrelevant. The nonlinear least squares problem is solved with Levenberg-Marquardt algorithm [67] and we will get a parameter set.

In order to refine the fit of finite nuclei data, the nonlinear least-squares minimization is performed one more time without including the data from the bulk properties of nuclear matter. Of course, in this way some deviations from empirical values of bulk properties are emerged. In that case, one needs to start from the beginning, and several repeats are necessary to reach the desired parameter set. Under the definition (21) we compared the productions of our parameter set with NL3 [68] and FSUGold [52] in Table I. The performances of our parameter set in finite nuclei and in the nuclear matter at the saturation density are as good as NL3 and FSUGold.

TABLE I. The third column contains the experimental/empirical values of finite nuclei data and the bulk properties of the nuclear matter, in brackets are the weights used in the fitting according to the definition (22).

	Nucl.	expt./emp.	This work	FSUGold	NL3
E_b/A (MeV)	^{40}Ca	−8.551(14.35)	−8.550	−8.54	−8.54
	^{48}Ca	−8.666(11.47)	−8.653	−8.58	−8.64
	^{208}Pb	−7.867(14.08)	−7.866	−7.89	−7.88
r_c (fm)	^{40}Ca	3.478(7.51)	3.437	3.42	3.46
	^{48}Ca	3.477(7.46)	3.453	3.45	3.46
	^{208}Pb	5.501(8.35)	5.522	5.52	5.51
ρ_0 (fm^{-3})		0.153(2.30)	0.146	0.148	0.148
E/A (MeV)		−16(2.99)	−16.19	−16.28	−16.24
K_0 (MeV)		250(2.30)	259	230	271
$E_{\rm sym}$ (MeV)		33(2.30)	36.1	32.6	37.4
χ^2 (%)		–	1.102	0.785	2.134

TABLE II. Comparison of our parameter set with the famous nonlinear meson coupling models FSUGold and NL3.

	This work	FSUGold	NL3
m_σ (MeV)	510.6780	491.5000	508.1941
g_2 (fm^{-1})	−4.5067	−4.2770	−10.4307
g_3	32.2796	49.8515	−28.8851
c_0	−241.1305	−418.39	
g_σ	10.6656	10.5924	10.2169
g_ω	13.8116	14.3020	12.8675
g_δ	4.2014		
g_ρ	5.3190	5.8837	4.4744
T_b		−1699.4	

The calibrated values of our parameter set, named as NLX8, are listed in Table II, as well as that of NL3 and FSUGold. Compared with FSUGold, the self-couplings of ω meson is weakened in the new fitted parameter set. The isospin dependence is described by ρ meson solely in NL3. In our model as well as FSUGold, the coupling constants of nucleon and ρ meson are larger than NL3, which means stronger symmetry energies. The mechanics of softening the symmetry energy is different in FSUGold and our model. The former is via the strong coupling between ρ meson and ω meson, while in the latter the softening is provided by the scalar-isovector δ meson.

IV. RESULTS AND DISCUSSIONS

A. Experimental and astrophysical constraints on the EoS

The only way one can compress nuclear matter to high density in a laboratory environment is by nuclear collisions. The EoS-sensitive observables have been deduced via analyzing the compression and expansion dynamics of the flow in energetic nuclear collisions [69]. This puts valuable constraints on the symmetric nuclear matter, which is illustrated in Fig. 1(a) as the area filled by crossed lines. In the pure neutron matter, additional pressure arises due to the existence of the repulsive symmetry energy. Therefore, the constraints on the pure neutron matter should account the pressures from asymmetry terms, namely $P_{\rm asy} \sim \rho^2 dE_{\rm sym}/d\rho$. By assuming strong and weak density dependence on the symmetry energy [70], the constraints on the pure neutron matter are obtained, as the area filled by 45° lines and the area filled by blank space in Fig. 1(b), respectively. The nuclear collision experiment seems to rule out the model NL3, which produces too much pressure both in the symmetric nuclear matter and in the pure neutron matter. Indeed, it is difficult for RMF models containing only self-couplings of σ meson to achieve good agreements in both symmetric nuclei and neutron-rich nuclei, without violating the constraints obtained by nuclear collisions. On the contrary, the parameter set FSUGold (abbreviated as FSU in Fig. 1 and following figures), which contains an additional self-coupling of ω meson produces less pressure. For the same reason, although our parameter set predicts a large compressibility ($K_0 = 259$ MeV) at the saturation density, the high-density behavior is largely

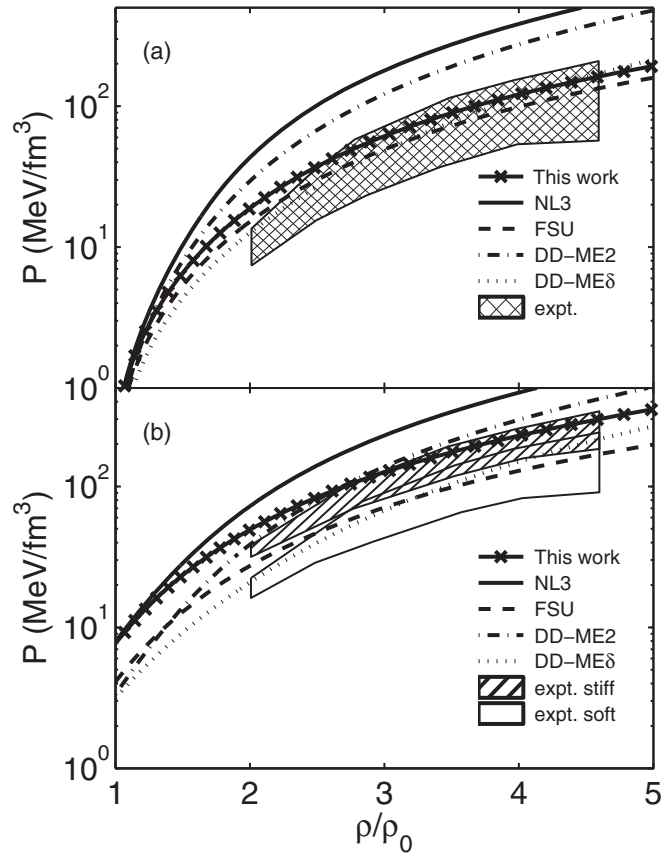

FIG. 1. (a) The pressures of the symmetric nuclear matter and (b) the pure neutron matter as functions of the scaled density ρ/ρ_0, where $\rho_0 \sim 2.7 \times 10^{14}g/cm^3 \approx 0.16$ fm^{-3}. The area filled with crossed lines in (a) corresponds to the region of pressures consistent with the experimental flow data. The areas filled with 45° lines and blank space in (b) correspond to constraints on the EoS after inclusion a stiff and a soft symmetry energy term, respectively.

improved and is consistent with the experimental flow data. The major differences of NL3, FSUGold, and our parameter set are the stiffness of the EoS of the symmetric matter in high-density area and the stiffness of the symmetry energy. In simple terms, the NL3 set predicts a stiff EoS for the symmetric nuclear matter and a stiff symmetry energy. On the contrary, the FSUGold set predicts a soft EoS for the symmetric nuclear matter at high density and a soft symmetry energy. Meanwhile, our parameter set predicts a soft EoS for symmetric nuclear matter but a stiff symmetry energy. In Fig. 1, we also draw the EoSs of DD-ME2 [71] and DD-MEδ [72], which are density-dependent meson-exchange models. They have flexible density-dependent couplings and usually predict softer symmetry energies than nonlinear RMF models.

In addition to the experimental data from nuclear collisions, our current knowledge about the matter in high-density condition mostly comes from the astrophysical observations. The EoS of the infinite nuclear matter is crucial to determine a lot of astrophysical phenomena, such as the radius and the mass of the neutron star (NS). In fact, once the EoS is given, solving the Tolman-Oppenheimer-Volkoff (TOV) equation

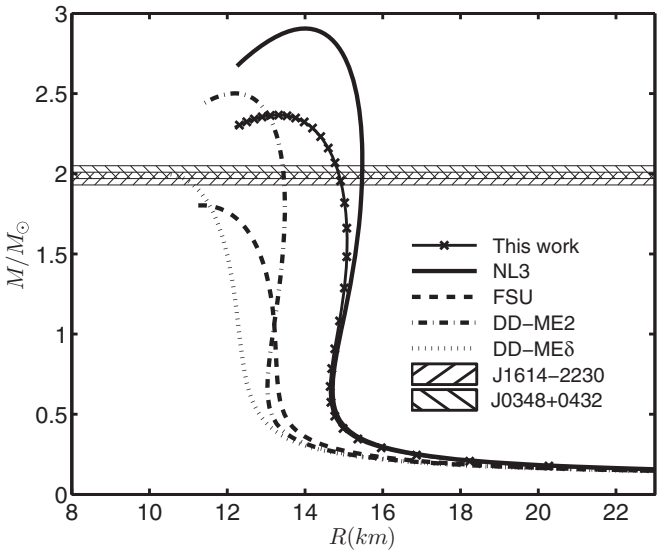

FIG. 2. The mass-radius relations predicted by several RMF parameter sets. Filled areas represent two neutron stars whose masses are precisely determined.

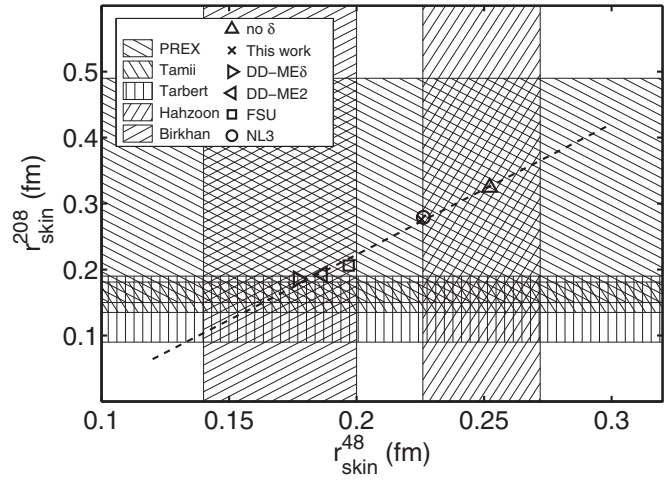

FIG. 3. Neutron skin thicknesses of ^{48}Ca and ^{208}Pb, predicted by several parameter sets. The filled areas are some constraints on the neutron skin thicknesses of ^{48}Ca (filled with 30° and 60° lines) and ^{208}Pb (filled with 90°, 120°, and 150° lines). The dashed line represents a linear fit of the theoretical predictions.

[73,74]

$$\frac{dP}{dr} = -\frac{Gm}{r^2}\rho\left(1+\frac{P}{\rho}\right)\left(1+\frac{4\pi r^3 P}{m}\right)\left(1-\frac{2Gm}{r}\right)^{-1},$$
$$\frac{dm}{dr} = 4\pi r^2 \rho, \tag{23}$$

we will get the mass and pressure distributions in a neutron star. Indeed, the maximum NS mass is mainly determined by the high-density behavior of the EoS, while the radius of a NS depends on how the crust is modeled [75]. For simplicity, in this work we use the BPS EoS [76] when the density is less than 0.08 fm^{-3}. The stiff parameter sets, which predict large pressure, such as NL3 and DD-ME2, produce larger NS maximum masses. On the contrary, the soft parameter sets DD-MEδ and FSUGold, especially the latter, produce a rather small NS maximum mass, as illustrated in Fig. 2. The maximum NS mass predicted by FSUGold is about 1.72 $M_\odot$ [52], where $M_\odot$ represents the solar mass. However, more massive NS have been precisely identified, e.g., PSR J0348+0432 with mass of 2.01 $\pm$ 0.04 $M_\odot$ [77] and PSR J1614-2230 with mass of 1.97 $\pm$ 0.04 $M_\odot$ [78]. They should be considered as the low bound of the theoretical prediction of the maximum NS mass. The new fitted parameter set is consistent with the constraint.

We found that the NS's radius is large in NL3 and our model, which produce stiff symmetry energies in high-density region. Meanwhile, the parameter sets with soft symmetry energies, such as FSUGold, DD-MEδ, and DD-ME2, predict small radii for NSs. Recently, important processes have been made in determining the radii of NSs, especially the binary neutron star merger event detected by LIGO-Virgo Collaboration [79] puts meaningful constraints on the tidal deformability, and leads to an upper limit about 13.76 km for a 1.4 $M_\odot$ NS [80]. But it does not necessarily rule out NL3 and our parameter set, because there are still many uncertainties remaining. In the core of massive NSs, hyperon mixtures [81,82], and quark matter [83,84] are speculated to emerge. The simple extrapolation of the nuclear models to the compact matter environment may be questionable. Fortunately, we notice that the radius of NS and the neutron skin thickness is closely related, the larger the neutron skin of the nucleus the larger the radius of the NS [85]. So scrutinizing the neutron skin thickness may provide more suitable insights to this question.

B. Neutron skin thickness

Unlike the proton density distribution that can be precisely measured via electron scattering, the direct measurement of the neutron density in a nucleus is difficult. Therefore, the evaluations of neutron skin thickness are typically indirect and model dependent. For example, theoretical analyses show that a strong correlation exists between the electric dipole polarizability α_D and the neutron skin thickness [86,87]. Based on it, the experimental measured electric dipole polarizabilities lead to a neutron skin thickness $0.156^{+0.025}_{-0.021}$ fm for ^{208}Pb [88] and 0.14–0.20 fm for ^{48}Ca [89]. Recently, alternative methods have been introduced and new results are carried out. Mahzoon *et al.* deduced a neutron skin of 0.249 $\pm$ 0.023 fm in ^{48}Ca from a nonlocal dispersive optical-model analysis [90]. The extraction of a neutron skin thickness from coherent pion photoproduction cross-section measurement, gives a value $0.15 \pm 0.03^{+0.01}_{-0.03}$ fm in ^{208}Pb [91]. The measurement of the neutron skin thickness of ^{208}Pb through parity violation (electroweak probe) in electron scattering gives a model-independent value $0.33^{+0.16}_{-0.18}$ fm, proposed by PREX Collaboration [92]. The various estimations are illustrated in Fig. 3 with lines in different directions. It is incompatible that for ^{48}Ca, the estimation by Birkhan *et al.* (30° lines) is significantly smaller than that by Hahzoon *et al.* (60° lines). As for ^{208}Pb, although the estimations by Tarbert *et al.* (90° lines) and Tamii *et al.* (120° lines) overlap with lead radius

experiment (PREX) proposal (150° lines), they are evidently smaller that the center value of PREX result 0.33 fm. In the same figure, we also depict the predictions by several RMF models, among which the No δ means removing the coupling of δ meson from our parameter set. The parameter set of this work predicts large neutron skin thicknesses both in ^{48}Ca and ^{208}Pb, which is similar to NL3. Because they all stand for a stiff symmetry energy. Just as expected, removal of the δ meson will make the neutron skin thickness even larger. On the other hand, the parameter sets predicting soft symmetry energies, like FSUGold, DD-ME2, and DD-MEδ, predict small neutron skin thicknesses. Hence it is still obscure that whether the neutron skin thickness is large or small. In fact, the authors of Ref. [93] tested theoretical models with various laboratory and observational data, and found it is premature to rule out models with large neutron skins. Nevertheless, it is clear to see that in RMF models the neutron skin of ^{48}Ca is proportional to that of ^{208}Pb, and a robust correlation exists:

$$r_{\rm skin}^{208} = 1.981 \times r_{\rm skin}^{48} - 0.174 \quad \text{(fm)}, \tag{24}$$

with a goodness of fit $R^2 = 0.986$. So besides pinning down the symmetry energy, determining both of the neutron thicknesses has a crucial meaning: to check to what extent the relativistic mean field treatments reflect the physical nuclear scenario. We expect more accurate results of the follow-up calcium radius experiment (CREX) and PREX-II experiment [94] by Jefferson Laboratory will make decisive conclusions on these problems.

C. Pygmy dipole resonance and neutron-proton effective mass splitting

In previous sections, we have verified the new calibrated parameter set with finite nuclear data and constraints from experimental measurements and astrophysical observations. In this section we will use it to investigate the low-lying response of a nucleus to external electric perturbations and focus on the effects caused by the scalar-isovector meson δ. The electric dipole excitations of ^{48}Ca and ^{208}Pb are calculated using the random phase approximation method, which are induced by the electric (isovector) dipole operator [95]

$$\hat{E}_{1\mu} = e \sum_i \left(\frac{N-Z}{2A} - t_3^i \right) r_i Y_{1\mu}. \tag{25}$$

It is well known that the theoretical evaluations of the electric dipole energy weighted sum rules (EWSR) are overestimated than the classical Thomas-Reiche-Kuhn (TRK) sum rules [95], due to the density-dependence and velocity-relating terms [30,87,96]. Therefore, in order to reconcile the experimental transition strengths, the calculated ones are divided by a factor 1.5 in Fig. 4. Meanwhile, the Lorentz smooth parameter is $\Gamma = 2$ MeV. The wide structures of GDR can be easily identified and good agreements with experimental results [88,89] are achieved both in ^{48}Ca and ^{208}Pb cases. As for PDR, we notice the experimental investigation [97] reported a value about 8.4 MeV for ^{48}Ca. However, in our calculations no corresponding resonance structures are found. On the contrary, significant low-lying excitations are confirmed in ^{208}Pb around the neutron emission energy.

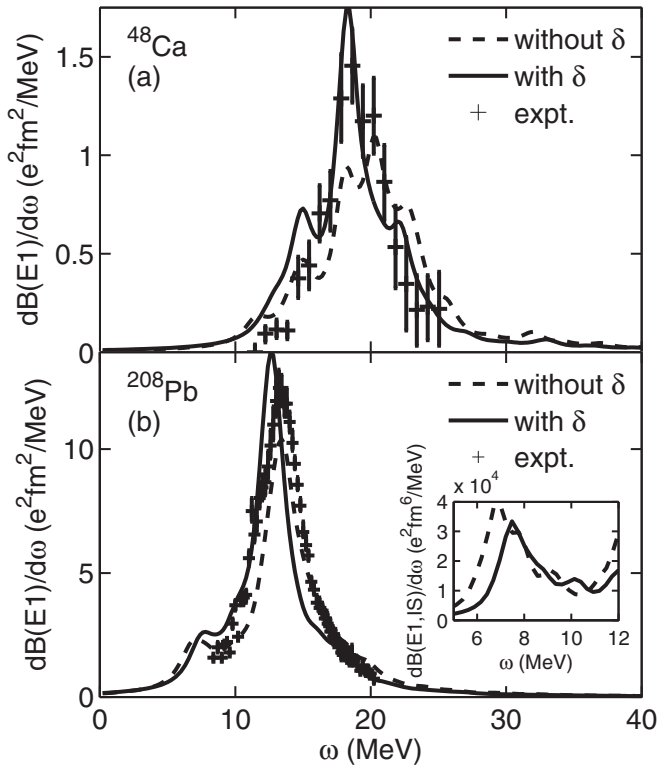

FIG. 4. The transition strength distribution of the electric dipole resonance in (a) ^{48}Ca and (b) ^{208}Pb, the smear width is $\Gamma = 2$ MeV. The inset represents the transition strengths of the isoscalar (IS) electric dipole operator. The theoretical results are scaled, see text for details.

In order to quantify the positions of the resonance peaks, we calculate the centroid energies of the distributions, which is defined as $E_c = m_1/m_0$. The strengths of PDR are integrated below the neutron emission threshold of ^{208}Pb to avoid the contribution from the low energy tail of GDR. To be specific, the centroid energy of PDR is calculated in the region $0 \sim 8$ MeV, and $8 \sim 30$ MeV for GDR. We also calculate the centroid energies of the whole distributions in the range $0 \sim 40$ MeV, labeled as Total. Strengths with excitation energies larger than 40 MeV contribute little to the results. The centroid energies are summarized in Table III. Excellent agreement between RPA calculated centroid energy and experimental result is achieved in GDR of ^{48}Ca, which are 18.74 MeV and 18.9(2) MeV [89], respectively. In ^{208}Pb, the positions of GDR peak and PDR peak, i.e., 13.18 MeV and 7.43 MeV, are also

TABLE III. The centroid energies (in MeV) of GDR and PDR in ^{48}Ca and ^{208}Pb, compared with experimental measurements.

	^{48}Ca			^{208}Pb		
	PDR	GDR	Total	PDR	GDR	Total
Full δ	–	18.74	19.04	7.43	13.18	12.81
Half δ	–	19.36	19.90	7.15	14.03	13.43
No δ	–	19.57	20.20	7.08	14.32	13.60
expt.	8.4	18.9(2)	–	7.37	13.3(1)	–

quite close to the experimental values 13.3(1) MeV [98] and 7.37 MeV [99].

PDR is different in many ways to GDR. Unlike the GDR, which is caused by the relative oscillation between neutrons and protons, PDR involves only the excess neutrons outside of the isospin saturated core. To identify the isospin character of the low-lying excitations, we also calculated the electric isoscalar (IS) dipole strength in ^{208}Pb. The corresponding operator is [100]

$$E^{\rm IS}_{1\mu} = e\sum_i \left(r_i^2 - \frac{5}{3}\langle r^2\rangle\right) r_i Y_{1\mu}. \tag{26}$$

As illustrated in the inset of Fig. 4(b), the low-lying excitation strengths are also aroused by the isoscalar probe, which centers at almost the same position as the isovector dipole excitations, i.e., the PDR. The explicit value of the centroid energy, if one integrates in the energy region $0 \sim 8$ MeV, is 7.41 MeV. The peak of the low-lying isoscalar electric dipole strength moves to 7.05 MeV if we switch off the interaction of δ meson. The coincidence of the peak positions of the low-lying isoscalar dipole resonance and PDR, as well as the similar shift of each peak in the absence of δ meson, are strong hints to the isoscalar predominance of the pygmy dipole resonance. This result is consistent with previous researches [39–41].

PDR is not as collective as GDR [31] and is highly sensitive to the structure of the neutron single-particle levels near the Fermi surface. Our calculation suggests the PDR of ^{208}Pb is mainly induced by the excitations of the neutrons in orbitals near the Fermi surface, such as $3p_{1/2}$, $3p_{3/2}$, and $2f_{5/2}$. In the framework of random phase approximation method, excitations of a nucleus are described by coherent 1p1h transitions. In a particular excitation state ν, the contribution from a 1p1h pair (p,h) with energy $\epsilon_{ph} = \epsilon_p - \epsilon_h$ can be measured by the coefficient

$$C^\nu_{ph} \equiv \left|X^\nu_{ph}\right|^2 - \left|Y^\nu_{ph}\right|^2, \tag{27}$$

which is normalized as $\sum_{ph} C^\nu_{ph} = 1$. Typically, in PDR region excitations are mainly caused by only a few 1p1h transitions. In Table IV we list the details of the dominant excited states in PDR, including the excited energies, transition probabilities, and 1p1h configurations. The block labeled as Full δ contains the results of our parameter set. The excitation state with energy 7.42 MeV is mainly caused by the transition of neutron pairs $3p_{1/2} \to 3d_{3/2}$ and $3p_{3/2} \to 3d_{5/2}$, which takes 62.4% and 10.1% of the whole contribution, respectively. Other configuration pairs only take very small fractions. Similarly, the excited state at 7.54 MeV is also dominated by a few 1p1h transitions, namely, 74.8% by $3p_{3/2} \to 3d_{5/2}$ and 12.1% by $3p_{1/2} \to 3d_{3/2}$. These results reveal the low-collectivity nature of PDR.

The δ meson, by its scalar-isovector nature, will make neutron single-particle levels lower and make proton levels higher. The shift of the single-particle levels via changing δ meson field is opposite to that caused by ρ meson. In order to focus on the effects caused by δ meson, we reduce the coupling constant g_δ and check how the spectrum changes. In the case Half δ we reduce the coupling constant of δ meson by half; and in the case No δ, we set it to 0. It should be mentioned that the interactions relating to δ meson must be adjusted in ground-state calculations and RPA calculations simultaneously. Otherwise, inconsistence is introduced and the low-lying states will be contaminated by translational spurious states [31,57]. When the coupling strength of δ meson is reduced, the energy gaps of 1p1h pairs that important to PDR is shrunk. For example, the energy of 1p1h transition $3p_{3/2} \to 3d_{5/2}$ changes from 7.63–7.08 MeV when the g_δ is reduced by half, and to 6.89 MeV when the δ meson is totally removed. The energies of 1p1h pairs that contribute most to PDR decrease with the reducing of δ meson coupling. Accordingly, the centroid energy of PDR decreases from 7.43 MeV (Full δ) to 7.15 MeV (Half δ) and 7.08 MeV (No δ). There is a clear tendency that the centroid energy of PDR in ^{208}Pb is lowered as the gaps are shrunk. On the contrary, the shift of GDR peak is opposite to PDR. The GDR is highly collective and the mechanism of the shift may be very different.

TABLE IV. The excited states that dominate in the pygmy dipole resonance of ^{208}Pb when δ meson is included (Full δ), reduced by half (Half δ), and excluded (No δ). The first and second columns contain the excited energies and transition probabilities of RPA states. For a particular state ν, the third column contains the 1p1h configurations (with energy ϵ_{ph} in the fourth column and ratio C_{ph} in the fifth column, N is a shorthand for neutron) that contribute most to the excited state ν.

ω_ν (MeV)	B_ν (e^2fm^2)	Conf.	ϵ_{ph} (MeV)	C_{ph} (%)
		Full δ		
7.42	0.972	[N] $3p_{1/2} \to 3d_{3/2}$	7.52	62.4
		[N] $3p_{3/2} \to 3d_{5/2}$	7.63	10.1
7.54	0.406	[N] $3p_{3/2} \to 3d_{5/2}$	7.63	74.8
		[N] $3p_{1/2} \to 3d_{3/2}$	7.52	12.1
		Half δ		
7.02	0.776	[N] $3p_{3/2} \to 3d_{5/2}$	7.08	83.9
7.92	0.571	[N] $2f_{5/2} \to 2g_{7/2}$	8.14	44.2
		[N] $2f_{7/2} \to 2g_{9/2}$	8.34	40.9
		No δ		
6.86	0.869	[N] $3p_{3/2} \to 3d_{5/2}$	6.89	83.6
7.82	0.475	[N] $2f_{5/2} \to 3d_{3/2}$	7.92	65.7
		[N] $2f_{5/2} \to 2g_{7/2}$	8.00	21.7

The δ meson, transmitting the nuclear force in the scalar-isovector channel, is sensitive to nuclear isospin asymmetry properties. As we have mentioned in previous sections, the inclusion of the scalar-isovector meson δ reduces the symmetry energy. On the contrary, removing δ meson from our calibrated parameter set makes the symmetry energy stiffer, as depicted in Fig. 5(a). The symmetry energy at the saturation density $E_{\rm sym}$ will increase by 23% when the δ meson is totally removed. Accordingly, the slope parameter of the symmetry energy $L_{\rm sym}$ will increase by 16% while the curvature parameter $K_{\rm sym}$ will decrease by about 80%. Meanwhile, our calculation shows when the coupling strength between nucleon and δ meson is reduced, the centroid energy of the whole

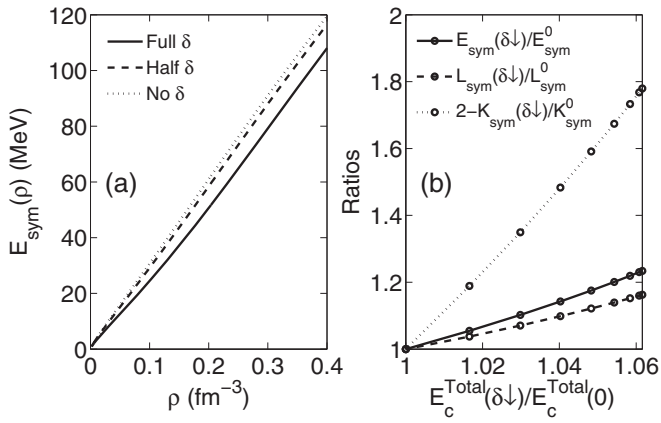

FIG. 5. (a) The symmetry energy predicted by our parameter set, in the cases of Full δ (solid line), Half δ (dashed line), and No δ (dotted line); (b) The relationships between the symmetry energy $E_{\rm sym}$ (solid line), the slope parameter $L_{\rm sym}$ (dashed line), and the curvature parameter $K_{\rm sym}$ (dotted line) at the saturation density and the centroid of the whole electric dipole strength $E_c^{\rm Total}$ in ^{208}Pb, when the coupling of δ meson is reduced ($\delta\downarrow$). The quantities labeled with 0 represent the results in the Full δ case.

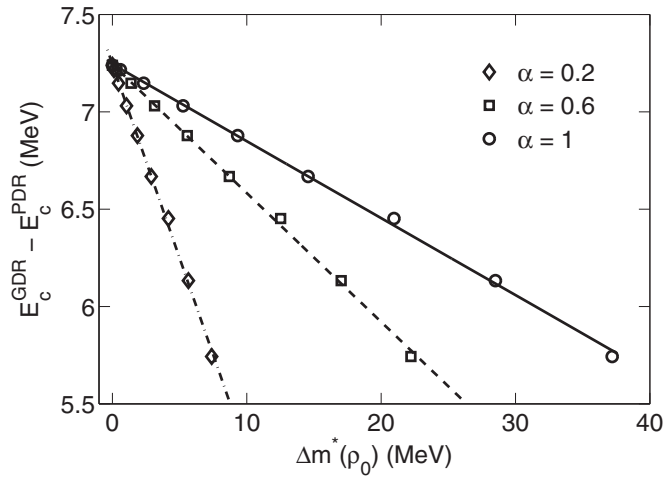

FIG. 6. The relationship between the neutron-proton effective mass splitting and the difference of the centroid energies of GDR and PDR in ^{208}Pb. The effective masses are evaluated at the saturation density ρ_0. The circles, squares, and diamonds denote the results in asymmetric matter with different neutron excess ratios. The lines are linear fits.

isovector electric dipole strength in ^{208}Pb will shift as large as 6%. From Fig. 5(b) we can see, the relationships between the symmetry energy as well as its slope and curvature parameters and the total centroid position ($E_c^{\rm Total}$) of the electric dipole excitations, by changing the δ meson solely, is slowly varying and smooth. Although deviations from linear correlations are significant, a positive correlation between the symmetry energy and the centroid of the electric dipole resonance can be established in the scalar-isovector channel.

In RMF models without the δ meson, the effective mass, as defined in (6), is the same for neutron and proton. Neutron-proton mass splitting is an effect peculiar to the δ meson. The interaction in the scalar-isovector channel dissimilate the Lorentz transformation properties of neutrons and protons. Whereas the total effective mass is roughly unchanged. Actually, all the RMF models we mentioned above, i.e., NL3, FSUGold, DD-ME2, DD-MEδ, as well as our parameter set, have similar nucleon effective masses, which are about 0.6 times of the bare nucleon masses. In the framework of the relativistic mean field theory, the parameter set with a too large or too small effective nucleon mass always fails to reproduce the finite nuclear data, such as masses and radii. Neither could it give proper descriptions to the nucleus excitation properties, such as low-lying resonances. In the relativistic mean field theory, the splitting of neutron-proton effective mass is negative ($m_n^* < m_p^*$) [101], and is determined by the coupling between nucleon and δ meson,

$$\Delta m^* = m_p^* - m_n^* = 2g_\delta \cdot \delta. \tag{28}$$

As we have learned from Table III, the coupling strength between nucleon and meson in the scalar-isovector channel affects the positions of GDR and PDR. In order to investigate the relationship between the neutron-proton mass splitting and the electric dipole resonance for further details, the coupling constant of δ meson is changed from 0 to g_δ with a step $\frac{1}{8}g_\delta$. We found the difference of GDR and PDR centroid energies in ^{208}Pb decreases linearly with the neutron-proton effective mass splitting at the saturation density. It should be noticed that in ^{208}Pb, the neutron excess ratio $(N-Z)/A \approx 0.21$. However, it is just an average value as the neutron and proton density distributions in a nucleus are not uniform. The asymmetry ratio may vary inside the nucleus or at the surface. Fortunately, as illustrated in Fig. 6, the linear correlation is robust and is valid for asymmetric matter with different neutron excess ratios ($\alpha \equiv (\rho_n - \rho_p)/\rho_B$). The overall fit of the relative offset of GDR and PDR peaks ΔE_c, the neutron-proton mass splitting Δm^* and the neutron excess ratio α reads

$$\Delta E_c = -0.0397 \times \frac{\Delta m^*}{\alpha} + 7.244 \quad \text{(MeV)}. \tag{29}$$

The formula (29) implies that the two electric dipole resonance structures, namely PDR and GDR, are not totally independent. Although different in formation, collectivity and isospin character, GDR and PDR are correlated by the isospin dependence of the asymmetric nuclear matter. The correlation maybe can provide us a new approach to determine the neutron-proton mass splitting.

V. CONCLUSIONS

The parameter set NLX8, which contains the nonlinear σ meson and ω meson self-couplings as well as the scalar-isovector meson δ, is carefully calibrated with finite nuclei data in this work. The parameter set is further constrained by terrestrial experimental measurements and astrophysical observations. As a model with nonlinear meson-exchange couplings, the EoS in high-density area is significantly improved and a sufficient NS maximum mass is guaranteed. The δ meson will soften the symmetry energy and reduce

the neutron skin thickness. With the carefully calibrated parameter set, we studied the electric dipole resonance in ^{48}Ca and ^{208}Pb. Good agreements with experimental measurements are achieved in both cases. The predominant isoscalar nature of PDR is confirmed by comparing PDR with the low-lying isoscalar electric dipole excitations. Our calculations show that in addition to affecting the symmetry energy and its density behavior, the strength of δ meson coupling also impacts the features of the electric dipole excitations significantly. The value of the symmetry energy and the centroid energy of the electric dipole resonance are positively correlated in the scalar-isovector channel. We found that by including the δ meson, the neutron single-particle levels near the Fermi surface are lowered. The energy gaps of 1p1h pairs that important to PDR are broadened. Due to the low collectivity nature, the pygmy dipole resonance is pushed higher. When the coupling strength of δ meson varies, the shifts of GDR peaks and PDR peaks are opposite. However, the relative offsets of GDR and PDR are predictable, which are closely correlated with the neutron-proton effective mass splitting, $\alpha \cdot \Delta E_c \sim \Delta m^*$. This may be helpful for understanding the behavior of the isospin dependence in asymmetric nuclear matter.

ACKNOWLEDGMENT

This work is partially supported by the Natural Science Foundation of Zhejiang Province under the Project No. LY19A050005.

[1] Y. Gambhir, P. Ring, and A. Thimet, Ann. Phys. (NY) **198**, 132 (1990).
[2] H. Müller and B. D. Serot, Nucl. Phys. A **606**, 508 (1996).
[3] J. Walecka, Ann. Phys. (NY) **83**, 491 (1974).
[4] M. Sharma, M. Nagarajan, and P. Ring, Phys. Lett. B **312**, 377 (1993).
[5] C. J. Horowitz and J. Piekarewicz, Phys. Rev. Lett. **86**, 5647 (2001).
[6] B. Liu, V. Greco, V. Baran, M. Colonna, and M. Di Toro, Phys. Rev. C **65**, 045201 (2002).
[7] D. P. Menezes and C. Providência, Phys. Rev. C **70**, 058801 (2004).
[8] Y. Zi and D. Wen-Bo, Chin. Phys. C **35**, 812 (2011).
[9] Z. Zhang and L.-W. Chen, Phys. Rev. C **93**, 034335 (2016).
[10] J. Rizzo, M. Colonna, and M. Di Toro, Phys. Rev. C **72**, 064609 (2005).
[11] B.-A. Li, Phys. Rev. C **69**, 064602 (2004).
[12] H.-Y. Kong, J. Xu, L.-W. Chen, B.-A. Li, and Y.-G. Ma, Phys. Rev. C **95**, 034324 (2017).
[13] B.-A. Li and L.-W. Chen, Mod. Phys. Lett. A **30**, 1530010 (2015).
[14] M. Jaminon and C. Mahaux, Phys. Rev. C **40**, 354 (1989).
[15] D. Peña-Arteaga, S. Goriely, and N. Chamel, Eur. Phys. J. A **52**, 320 (2016).
[16] D. Vretenar, T. Nikšić, and P. Ring, Phys. Rev. C **65**, 024321 (2002).
[17] S. Stringari, Phys. Lett. B **108**, 232 (1982).
[18] L. Trippa, G. Colò, and E. Vigezzi, Phys. Rev. C **77**, 061304 (2008).
[19] A. Carbone, G. Colò, A. Bracco, L.-G. Cao, P. F. Bortignon, F. Camera, and O. Wieland, Phys. Rev. C **81**, 041301 (2010).
[20] A. Klimkiewicz, N. Paar, P. Adrich, M. Fallot, K. Boretzky, T. Aumann, D. Cortina-Gil, U. Datta Pramanik, T. W. Elze, H. Emling, H. Geissel, M. Hellström, K. L. Jones, J. V. Kratz, R. Kulessa, C. Nociforo, R. Palit, H. Simon, G. Surówka, K. Sümmerer, D. Vretenar, and W. Waluś (LAND Collaboration), Phys. Rev. C **76**, 051603 (2007).
[21] J. Endres, D. Savran, P. A. Butler, M. N. Harakeh, S. Harissopulos, R.-D. Herzberg, R. Krücken, A. Lagoyannis, E. Litvinova, N. Pietralla, V.Y. Ponomarev, L. Popescu, P. Ring, M. Scheck, F. Schlüter, K. Sonnabend, V. I. Stoica, H. J. Wörtche, and A. Zilges, Phys. Rev. C **85**, 064331 (2012).
[22] P. Adrich, A. Klimkiewicz, M. Fallot, K. Boretzky, T. Aumann, D. Cortina-Gil, U. Datta Pramanik, T. W. Elze, H. Emling, H. Geissel, M. Hellström, K. L. Jones, J. V. Kratz, R. Kulessa, Y. Leifels, C. Nociforo, R. Palit, H. Simon, G. Surówka, K. Sümmerer, and W. Waluś (LAND-FRS Collaboration), Phys. Rev. Lett. **95**, 132501 (2005).
[23] N. Tsoneva and H. Lenske, Prog. Part. Nucl. Phys. **59**, 317 (2007), International Workshop on Nuclear Physics 28th Course.
[24] N. Tsoneva and H. Lenske, Phys. Rev. C **77**, 024321 (2008).
[25] R. Schwengner, G. Rusev, N. Tsoneva, N. Benouaret, R. Beyer, M. Erhard, E. Grosse, A. R. Junghans, J. Klug, K. Kosev, H. Lenske, C. Nair, K. D. Schilling, and A. Wagner, Phys. Rev. C **78**, 064314 (2008).
[26] D. Savran, T. Aumann, and A. Zilges, Prog. Part. Nucl. Phys. **70**, 210 (2013).
[27] D. Vretenar, N. Paar, T. Marketin, and P. Ring, J. Phys. G: Nucl. Part. Phys. **35**, 014039 (2008).
[28] C. Iwamoto, H. Utsunomiya, A. Tamii, H. Akimune, H. Nakada, T. Shima, T. Yamagata, T. Kawabata, Y. Fujita, H. Matsubara, Y. Shimbara, M. Nagashima, T. Suzuki, H. Fujita, M. Sakuda, T. Mori, T. Izumi, A. Okamoto, T. Kondo, B. Bilgier, H. C. Kozer, Y.-W. Lui, and K. Hatanaka, Phys. Rev. Lett. **108**, 262501 (2012).
[29] S. Goriely, Phys. Lett. B **436**, 10 (1998).
[30] T. Inakura, T. Nakatsukasa, and K. Yabana, Phys. Rev. C **84**, 021302 (2011).
[31] X.-W. Sun, J. Chen, and D.-H. Lu, Chin. Phys. C **42**, 014101 (2018).
[32] D. Vretenar, N. Paar, P. Ring, and G. Lalazissis, Nucl. Phys. A **692**, 496 (2001).
[33] J. Piekarewicz, Phys. Rev. C **73**, 044325 (2006).
[34] O. Wieland and A. Bracco, Prog. Part. Nucl. Phys. **66**, 374 (2011), particle and Nuclear Astrophysics.
[35] V. Baran, M. Colonna, M. Di Toro, A. Croitoru, and D. Dumitru, Phys. Rev. C **88**, 044610 (2013).
[36] K. Yoshida, Phys. Rev. C **80**, 044324 (2009).
[37] X. Sun, J. Chen, and D. Lu, Phys. Rev. C **98**, 024607 (2018).
[38] J. Endres, E. Litvinova, D. Savran, P. A. Butler, M. N. Harakeh, S. Harissopulos, R.-D. Herzberg, R. Krücken, A. Lagoyannis, N. Pietralla, V. Y. Ponomarev, L. Popescu, P. Ring, M. Scheck, K. Sonnabend, V. I. Stoica, H. J. Wörtche, and A. Zilges, Phys. Rev. Lett. **105**, 212503 (2010).

[39] X. Roca-Maza, G. Pozzi, M. Brenna, K. Mizuyama, and G. Colò, Phys. Rev. C **85**, 024601 (2012).

[40] H. Zheng, S. Burrello, M. Colonna, and V. Baran, Phys. Rev. C **94**, 014313 (2016).

[41] M. Urban, Phys. Rev. C **85**, 034322 (2012).

[42] J. Endres, D. Savran, A. M. van den Berg, P. Dendooven, M. Fritzsche, M. N. Harakeh, J. Hasper, H. J. Wörtche, and A. Zilges, Phys. Rev. C **80**, 034302 (2009).

[43] N. Paar, Y. F. Niu, D. Vretenar, and J. Meng, Phys. Rev. Lett. **103**, 032502 (2009).

[44] E. G. Lanza, A. Vitturi, E. Litvinova, and D. Savran, Phys. Rev. C **89**, 041601 (2014).

[45] D. Savran, M. Fritzsche, J. Hasper, K. Lindenberg, S. Müller, V. Y. Ponomarev, K. Sonnabend, and A. Zilges, Phys. Rev. Lett. **100**, 232501 (2008).

[46] O. Wieland, A. Bracco, F. Camera, G. Benzoni, N. Blasi, S. Brambilla, F. C. L. Crespi, S. Leoni, B. Million, R. Nicolini, A. Maj, P. Bednarczyk, J. Grebosz, M. Kmiecik, W. Meczynski, J. Styczen, T. Aumann, A. Banu, T. Beck, F. Becker, L. Caceres, P. Doornenbal, H. Emling, J. Gerl, H. Geissel, M. Gorska, O. Kavatsyuk, M. Kavatsyuk, I. Kojouharov, N. Kurz, R. Lozeva, N. Saito, T. Saito, H. Schaffner, H. J. Wollersheim, J. Jolie, P. Reiter, N. Warr, G. deAngelis, A. Gadea, D. Napoli, S. Lenzi, S. Lunardi, D. Balabanski, G. LoBianco, C. Petrache, A. Saltarelli, M. Castoldi, A. Zucchiatti, J. Walker, and A. Bürger, Phys. Rev. Lett. **102**, 092502 (2009).

[47] D. M. Rossi, P. Adrich, F. Aksouh, H. Alvarez-Pol, T. Aumann, J. Benlliure, M. Böhmer, K. Boretzky, E. Casarejos, M. Chartier, A. Chatillon, D. Cortina-Gil, U. Datta Pramanik, H. Emling, O. Ershova, B. Fernandez-Dominguez, H. Geissel, M. Gorska, M. Heil, H. T. Johansson, A. Junghans, A. Kelic-Heil, O. Kiselev, A. Klimkiewicz, J. V. Kratz, R. Krücken, N. Kurz, M. Labiche, T. Le Bleis, R. Lemmon, Y. A. Litvinov, K. Mahata, P. Maierbeck, A. Movsesyan, T. Nilsson, C. Nociforo, R. Palit, S. Paschalis, R. Plag, R. Reifarth, D. Savran, H. Scheit, H. Simon, K. Sümmerer, A. Wagner, W. Waluś, H. Weick, and M. Winkler, Phys. Rev. Lett. **111**, 242503 (2013).

[48] M. Scheck, S. Mishev, V. Y. Ponomarev, R. Chapman, L. P. Gaffney, E. T. Gregor, N. Pietralla, P. Spagnoletti, D. Savran, and G. S. Simpson, Phys. Rev. Lett. **116**, 132501 (2016).

[49] B. Löher, D. Savran, T. Aumann, J. Beller, M. Bhike, N. Cooper, V. Derya, M. Duchêne, J. Endres, A. Hennig, P. Humby, J. Isaak, J. Kelley, M. Knörzer, N. Pietralla, V. Ponomarev, C. Romig, M. Scheck, H. Scheit, J. Silva, A. Tonchev, W. Tornow, F. Wamers, H. Weller, V. Werner, and A. Zilges, Phys. Lett. B **756**, 72 (2016).

[50] J. Boguta and S. Moszkowski, Nucl. Phys. A **403**, 445 (1983).

[51] Y. Sugahara and H. Toki, Nucl. Phys. A **579**, 557 (1994).

[52] B. G. Todd-Rutel and J. Piekarewicz, Phys. Rev. Lett. **95**, 122501 (2005).

[53] P. Ring, Y. Gambhir, and G. Lalazissis, Comput. Phys. Commun. **105**, 77 (1997).

[54] Z. Ma, N. Van Giai, H. Toki, and M. L'Huillier, Phys. Rev. C **55**, 2385 (1997).

[55] D. Vretenar, A. Wandelt, and P. Ring, Phys. Lett. B **487**, 334 (2000).

[56] P. Ring, Z. Yu Ma, N. V. Giai, D. Vretenar, A. Wandelt, and L. Gang Cao, Nucl. Phys. A **694**, 249 (2001).

[57] D. Pena Arteaga and P. Ring, Phys. Rev. C **77**, 034317 (2008).

[58] J. Terasaki and J. Engel, Phys. Rev. C **82**, 034326 (2010).

[59] T. Nakatsukasa, T. Inakura, and K. Yabana, Phys. Rev. C **76**, 024318 (2007).

[60] H. Liang, T. Nakatsukasa, Z. Niu, and J. Meng, Phys. Rev. C **87**, 054310 (2013).

[61] M. Kortelainen, N. Hinohara, and W. Nazarewicz, Phys. Rev. C **92**, 051302 (2015).

[62] X. Sun and D. Lu, Phys. Rev. C **96**, 024614 (2017).

[63] P. Ring and P. Schuck, *The Nuclear Many-Body Problem* (Springer, Berlin, 2004).

[64] G. Audi, A. Wapstra, and C. Thibault, Nucl. Phys. A **729**, 337 (2003).

[65] I. Angeli and K. Marinova, At. Data Nucl. Data Tables **99**, 69 (2013).

[66] G. Lalazissis, S. Karatzikos, R. Fossion, D. P. Arteaga, A. Afanasjev, and P. Ring, Phys. Lett. B **671**, 36 (2009).

[67] D. Marquardt, J. Soc. Ind. Appl. Math. **11**, 431 (1963).

[68] G. A. Lalazissis, J. König, and P. Ring, Phys. Rev. C **55**, 540 (1997).

[69] P. Danielewicz, R. Lacey, and W. G. Lynch, Science **298**, 1592 (2002).

[70] N. K. Glendenning, F. Weber, and S. A. Moszkowski, Phys. Rev. C **45**, 844 (1992).

[71] G. A. Lalazissis, T. Nikšić, D. Vretenar, and P. Ring, Phys. Rev. C **71**, 024312 (2005).

[72] X. Roca-Maza, X. Viñas, M. Centelles, P. Ring, and P. Schuck, Phys. Rev. C **84**, 054309 (2011).

[73] R. C. Tolman, Phys. Rev. **55**, 364 (1939).

[74] J. R. Oppenheimer and G. M. Volkoff, Phys. Rev. **55**, 374 (1939).

[75] M. Fortin, C. Providência, A. R. Raduta, F. Gulminelli, J. L. Zdunik, P. Haensel, and M. Bejger, Phys. Rev. C **94**, 035804 (2016).

[76] G. Baym, C. Pethick, and P. Sutherland, Astrophys. J. **170**, 299 (1971).

[77] J. Antoniadis, P. C. C. Freire, N. Wex, T. M. Tauris, R. S. Lynch, M. H. van Kerkwijk, M. Kramer, C. Bassa, V. S. Dhillon, T. Driebe, J. W. T. Hessels, V. M. Kaspi, V. I. Kondratiev, N. Langer, T. R. Marsh, M. A. McLaughlin, T. T. Pennucci, S. M. Ransom, I. H. Stairs, J. van Leeuwen, J. P. W. Verbiest, and D. G. Whelan, Science **340**, 1233232 (2013).

[78] P. B. Demorest, T. Pennucci, S. M. Ransom, M. S. E. Roberts, and J. W. T. Hessels, Nature **467**, 1081 (2010).

[79] B.P. Abbott *et al.* (LIGO Scientific Collaboration and Virgo Collaboration), Phys. Rev. Lett. **119**, 161101 (2017).

[80] F. J. Fattoyev, J. Piekarewicz, and C. J. Horowitz, Phys. Rev. Lett. **120**, 172702 (2018).

[81] N. K. Glendenning and S. A. Moszkowski, Phys. Rev. Lett. **67**, 2414 (1991).

[82] N. K. Glendenning, Phys. Lett. B **114**, 392 (1982).

[83] H. Heiselberg, C. J. Pethick, and E. F. Staubo, Phys. Rev. Lett. **70**, 1355 (1993).

[84] A. Akmal, V. R. Pandharipande, and D. G. Ravenhall, Phys. Rev. C **58**, 1804 (1998).

[85] C. J. Horowitz and J. Piekarewicz, Phys. Rev. C **64**, 062802 (2001).

[86] P.-G. Reinhard and W. Nazarewicz, Phys. Rev. C **81**, 051303 (2010).

[87] J. Piekarewicz, Phys. Rev. C **83**, 034319 (2011).

[88] A. Tamii, I. Poltoratska, P. von Neumann-Cosel, Y. Fujita, T. Adachi, C. A. Bertulani, J. Carter, M. Dozono, H. Fujita, K. Fujita, K. Hatanaka, D. Ishikawa, M. Itoh, T. Kawabata, Y.

Kalmykov, A. M. Krumbholz, E. Litvinova, H. Matsubara, K. Nakanishi, R. Neveling, H. Okamura, H. J. Ong, B. Özel-Tashenov, V. Y. Ponomarev, A. Richter, B. Rubio, H. Sakaguchi, Y. Sakemi, Y. Sasamoto, Y. Shimbara, Y. Shimizu, F. D. Smit, T. Suzuki, Y. Tameshige, J. Wambach, R. Yamada, M. Yosoi, and J. Zenihiro, Phys. Rev. Lett. **107**, 062502 (2011).

[89] J. Birkhan, M. Miorelli, S. Bacca, S. Bassauer, C. A. Bertulani, G. Hagen, H. Matsubara, P. von Neumann-Cosel, T. Papenbrock, N. Pietralla, V. Y. Ponomarev, A. Richter, A. Schwenk, and A. Tamii, Phys. Rev. Lett. **118**, 252501 (2017).

[90] M. H. Mahzoon, M. C. Atkinson, R. J. Charity, and W. H. Dickhoff, Phys. Rev. Lett. **119**, 222503 (2017).

[91] C. M. Tarbert, D. P. Watts, D. I. Glazier, P. Aguar, J. Ahrens, J. R. M. Annand, H. J. Arends, R. Beck, V. Bekrenev, B. Boillat, A. Braghieri, D. Branford, W. J. Briscoe, J. Brudvik, S. Cherepnya, R. Codling, E. J. Downie, K. Foehl, P. Grabmayr, R. Gregor, E. Heid, D. Hornidge, O. Jahn, V. L. Kashevarov, A. Knezevic, R. Kondratiev, M. Korolija, M. Kotulla, D. Krambrich, B. Krusche, M. Lang, V. Lisin, K. Livingston, S. Lugert, I. J. D. MacGregor, D. M. Manley, M. Martinez, J. C. McGeorge, D. Mekterovic, V. Metag, B. M. K. Nefkens, A. Nikolaev, R. Novotny, R. O. Owens, P. Pedroni, A. Polonski, S. N. Prakhov, J. W. Price, G. Rosner, M. Rost, T. Rostomyan, S. Schadmand, S. Schumann, D. Sober, A. Starostin, I. Supek, A. Thomas, M. Unverzagt, T. Walcher, L. Zana, and F. Zehr (Crystal Ball at MAMI and A2 Collaboration), Phys. Rev. Lett. **112**, 242502 (2014).

[92] S. Abrahamyan, Z. Ahmed, H. Albataineh, K. Aniol, D. S. Armstrong, W. Armstrong, T. Averett, B. Babineau, A. Barbieri, V. Bellini, R. Beminiwattha, J. Benesch, F. Benmokhtar, T. Bielarski, W. Boeglin, A. Camsonne, M. Canan, P. Carter, G. D. Cates, C. Chen, J.-P. Chen, O. Hen, F. Cusanno, M. M. Dalton, R. De Leo, K. de Jager, W. Deconinck, P. Decowski, X. Deng, A. Deur, D. Dutta, A. Etile, D. Flay, G. B. Franklin, M. Friend, S. Frullani, E. Fuchey, F. Garibaldi, E. Gasser, R. Gilman, A. Giusa, A. Glamazdin, J. Gomez, J. Grames, C. Gu, O. Hansen, J. Hansknecht, D. W. Higinbotham, R. S. Holmes, T. Holmstrom, C. J. Horowitz, J. Hoskins, J. Huang, C. E. Hyde, F. Itard, C.-M. Jen, E. Jensen, G. Jin, S. Johnston, A. Kelleher, K. Kliakhandler, P. M. King, S. Kowalski, K. S. Kumar, J. Leacock, J. Leckey, J. H. Lee, J. J. LeRose, R. Lindgren, N. Liyanage, N. Lubinsky, J. Mammei, F. Mammoliti, D. J. Margaziotis, P. Markowitz, A. McCreary, D. McNulty, L. Mercado, Z.-E. Meziani, R. W. Michaels, M. Mihovilovic, N. Muangma, C. Muñoz Camacho, S. Nanda, V. Nelyubin, N. Nuruzzaman, Y. Oh, A. Palmer, D. Parno, K. D. Paschke, S. K. Phillips, B. Poelker, R. Pomatsalyuk, M. Posik, A. J. R. Puckett, B. Quinn, A. Rakhman, P. E. Reimer, S. Riordan, P. Rogan, G. Ron, G. Russo, K. Saenboonruang, A. Saha, B. Sawatzky, A. Shahinyan, R. Silwal, S. Sirca, K. Slifer, P. Solvignon, P. A. Souder, M. L. Sperduto, R. Subedi, R. Suleiman, V. Sulkosky, C. M. Sutera, W. A. Tobias, W. Troth, G. M. Urciuoli, B. Waidyawansa, D. Wang, J. Wexler, R. Wilson, B. Wojtsekhowski, X. Yan, H. Yao, Y. Ye, Z. Ye, V. Yim, L. Zana, X. Zhan, J. Zhang, Y. Zhang, X. Zheng, and P. Zhu (PREX Collaboration), Phys. Rev. Lett. **108**, 112502 (2012).

[93] F. J. Fattoyev and J. Piekarewicz, Phys. Rev. Lett. **111**, 162501 (2013).

[94] R. Michaels, arXiv:1510.04592v2.

[95] B. R. Mottelson and A. N. Bohr, *Nuclear Structure 2 Volume Set* (World Scientific, Singapore, 1998).

[96] M. N. Harakeh and A. van der Woude, *Giant Resonances: Fundamental High-Frequency Modes of Nuclear Excitation* (Oxford University Press, Oxford, 2001).

[97] T. Hartmann, M. Babilon, S. Kamerdzhiev, E. Litvinova, D. Savran, S. Volz, and A. Zilges, Phys. Rev. Lett. **93**, 192501 (2004).

[98] J. Ritman, F.-D. Berg, W. Kühn, V. Metag, R. Novotny, M. Notheisen, P. Paul, M. Pfeiffer, O. Schwalb, H. Löhner, L. Venema, A. Gobbi, N. Herrmann, K. D. Hildenbrand, J. Mösner, R. S. Simon, K. Teh, J. P. Wessels, and T. Wienold, Phys. Rev. Lett. **70**, 533 (1993).

[99] N. Ryezayeva, T. Hartmann, Y. Kalmykov, H. Lenske, P. von Neumann-Cosel, V. Y. Ponomarev, A. Richter, A. Shevchenko, S. Volz, and J. Wambach, Phys. Rev. Lett. **89**, 272502 (2002).

[100] N. V. Giai and H. Sagawa, Nucl. Phys. A **371**, 1 (1981).

[101] E. N. E. van Dalen, C. Fuchs, and A. Faessler, Phys. Rev. Lett. **95**, 022302 (2005).